Supplementary Information for:

Growth of curved crystals: competition between topological defect nucleation and boundary branching

Long Ma [a,§], *Xuepeng Liu* [ab,§], *Ai-kah Soh* [c,], *Linghui He* [a], *Changzheng Wu* [d], *and Yong Ni* [a*]

a CAS Key Laboratory of Mechanical Behavior and Design of Materials, Department of Modern Mechanics, University of Science and Technology of China, Hefei, Anhui 230026, P. R. China
b Anhui Province Key Lab of Aerospace Structural Parts Forming Technology and Equipment, Institute of Industry and Equipment Technology, Hefei University of Technology, Hefei, Anhui 230009, P. R. China
c School of Engineering, Monash University Malaysia, Jalan Lagoon Selatan, Bandar Sunway, Selangor Darul Ehsan, 47500, Malaysia
d Division of Nanomaterials & Chemistry, Hefei National Laboratory for Physical Sciences at the Microscale, University of Science and Technology of China, Hefei, Anhui 230026, P. R. China

1. The criteria of boundary instability in crystal sheet on spherical substrate

Firstly we assume that the boundary of circular crystal sheet experiences a small periodic perturbation:

$$r\left(\theta\right)=W+a_n\cos n\theta\,, \tag{S1}$$

where W is the initial radius of the circular sheet, a_n is the amplitude of the small perturbation with $a_n/W =$ 1, and $n\geq 2$ is an integer represent the azimuthal wave number. The total chemical potential μ of the crystal sheet is given by[3]

$$\mu=\mu_0+\Omega\left[\gamma C\left(\theta\right)+E_e\left(\theta\right)\right], \tag{S2}$$

where μ_0 is the undisturbed chemical potential far from the boundary and Ω is the surface area. γ is the edge energy per unit length of the boundary, which mainly consists of the adhesive energy and generates the boundary force. $C\left(\theta\right)$ and $E_e\left(\theta\right)$ are the curvature and the elastic energy per unit area at the perimeter. After the perturbation the stress function $\chi\left(r,\theta\right)$ has the general form: [4]

$$\chi\left(r,\theta\right)=\chi\left(r\right)+a_n\left(\alpha_n r^{n+2}+\beta_n r^n\right)\cos n\theta\,, \tag{S3}$$

where $\chi\left(r\right)$ is the stress function far from the perturbed edge and is independent of azimuthal angle θ,

α_n and β_n are undetermined coefficients which can be defined by the boundary conditions:

$$\sigma_{ij} n_j = -\gamma C(\theta) n_i \tag{S4}$$

with $\mathbf{n} \approx \mathbf{r} + \boldsymbol{\theta}(a_n/W) n \sin n\theta$ to the first order of a_n/W. For the given perturbation form as Eq. (S8) shows, the curvature can be expressed as

$$C(\theta) \approx (1/W)\left[1 + \left(n^2 - 1\right)\left(a_n/W\right)\cos n\theta\right], \tag{S5}$$

then the coefficients α_n and β_n which satisfy the boundary conditions Eq. (S4) can be determined and the Airy stress function is shown as[4]

$$\begin{aligned} \chi(r,\theta) = \chi(r) - \frac{1}{2} a_n \frac{\sigma_{\theta\theta}^0(W)}{W} (r/W)^n \left(r^2 - W^2\right)\cos n\theta \\ - a_n \frac{\gamma}{2W^2} (r/W)^n \left[(n-1)r^2 - (n+1)W^2\right]\cos n\theta \end{aligned}, \tag{S6}$$

where $\sigma_{\theta\theta}^0(W)$ is the hoop stress in the absence of boundary perturbation. The stress-redistribution induced by boundary perturbation consists of two parts: the elastic energy of crystal sheet and the work of boundary force. In the range of $\gamma/W >> \sigma_{\theta\theta}^0(W)$, the second term in Eq. (S6) of stress function can be neglected. It means that in the case of edge energy dominates, the radial stress at the perimeter stretches the crystal sheet and the boundary is always stable. On the contrary, when $\gamma/W = \sigma_{\theta\theta}^0(W)$, the elastic energy density along the perimeter is

$$\begin{aligned} E_e &\approx \left[\sigma_{\theta\theta}\left(W + a_n \cos n\theta\right)\right]^2 / 2Y \approx \left[\sigma_{\theta\theta}^0\left(W + a_n \cos n\theta\right) - (2n+1)\sigma_{\theta\theta}^0(W)\frac{a_n}{W}\cos n\theta\right]^2 \Big/ 2Y \\ &\approx \frac{1}{2Y}\left\{\left[\sigma_{\theta\theta}^0(W)\right]^2 + W\frac{d}{dr}\left[\sigma_{\theta\theta}^0(W)\right]^2 \frac{a_n}{W}\cos n\theta - (2n+1)\left[\sigma_{\theta\theta}^0(W)\right]^2 \frac{a_n}{W}\cos n\theta\right\} \end{aligned}, \tag{S7}$$

It is worth noting that although the stress function includes the contribution of surface elasticity, but in the limit of $\gamma/W = \sigma_{\theta\theta}^0(W)$, the elastic energy only contain the part of geometrical frustration induced stress. So the total chemical potential along the perturbed boundary can be expressed by

$$\mu(\theta)\approx\tilde{\mu}_0+\Omega\left\{\frac{\gamma}{W}\left(n^2-1\right)-\frac{1}{Y}\left\{(2n+1)\left[\sigma_{\theta\theta}^0(W)\right]^2-\frac{W}{2}\frac{d}{dr}\left[\sigma_{\theta\theta}^0(W)\right]^2\right\}\right\}\frac{a_n}{W}\cos n\theta, \qquad \text{(S8)}$$

where $\tilde{\mu}_0\approx\mu_0+\gamma\Omega/W+(\Omega/2Y)\left[\sigma_{\theta\theta}^0(W)\right]^2$ with Y the 2D Young's modulus. To evaluate the stability of the given perturbation, the atomic flux driven by the chemical potential gradient along the perimeter is $J=-\frac{M}{W}\frac{\partial\mu}{\partial\theta}$, where $M=D_s\delta_s/\Omega kT$ is the mobility with D_s the surface diffusivity, δ_s the atom number per unit area and kT the thermal energy. By substituting $\sigma_{\theta\theta}^0(W)=-YW^2/8R^2$ into Eq. (S7), the normal velocity of the perimeter can be express by the atomic flux as

$$v_n=-\frac{\Omega}{W}\frac{\partial J}{\partial\theta}=-\frac{\Omega^2M}{W^2}\left[\left(n^2-1\right)\frac{\gamma}{W}-(n-1)\frac{Y}{32}\left(\frac{W}{R}\right)^4\right]\frac{a_n}{W}\cos n\theta. \qquad \text{(S9)}$$

Considering the perturbation form Eq. (S1), we can obtain that

$$v_n=\frac{\partial r(\theta)}{\partial t}=\frac{\partial a_n}{\partial t}\cos n\theta. \qquad \text{(S10)}$$

Comparing Eqs. (S9) and (S10), the perturbation can be expressed as

$$a_n(t)=a_n(0)e^{t/\tau}, \qquad \text{(S11)}$$

where

$$\tau=-\frac{W^3}{\Omega^2Mn^2}\left[\left(n^2-1\right)\frac{\gamma}{W}-(n-1)\frac{Y}{32}\left(\frac{W}{R}\right)^4\right]^{-1}. \qquad \text{(S12)}$$

From Eqs. (S11) and (S12) one can see that $\tau>0$ means that the perturbation amplitude grows with the time, while $\tau<0$ means that the perturbation diminishes with the time. So the first term in bracket of Eq. (S12) denotes that the edge energy suppresses the boundary instability of crystal sheet and the circular sheet is energetically stable. In contrast, the second term of elastic energy is energetically favorable for the boundary instability. The competition between edge energy and elastic energy regulates the stability of the crystal sheet's perimeter. The critical condition of boundary instability is can be obtained from $\tau=0$ that

$$\frac{\gamma_n}{RY} \approx \frac{1}{32(n+1)} \left(\frac{W}{R} \right)^5 . \tag{S13}$$

2. The material properties of curved crystalline cap in BD simulation

Employing the stress expressions Eqs. (2)(3) and the stress which is calculated by relaxing a cap at zero temperature until its energy reaches the minimum value, the Young's modulus and edge energy of curved crystal are fitted with least-squares. Figure S1 shows the relationship between fitted Young's modulus Y versus different curvature radii R/a at fixed crystal size $W/R = 0.3$ and LJ potential strength $|U_0| = 3.5K_BT$. The Figure S2 shows the positive correlation between Y and $|U_0|$ at $R/a = 40$ and $W/R = 0.3$. As a comparison, the results of Young's modulus from simulated stress-strain curve are also plotted in Figure S2. Figure S1 and Figure S2 verify that the material properties from fitting method are credible in spite of the numerical deviation.

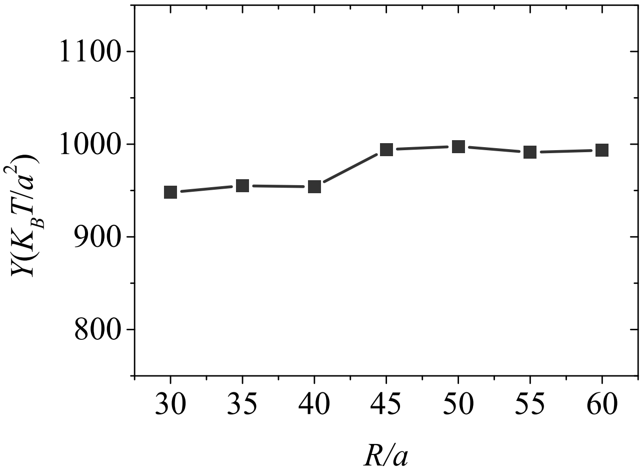

Figure S1 The relationship between fitted Young's modulus Y versus different curvature radii R/a at fixed crystal size $W/R = 0.3$ and LJ potential strength $|U_0| = 3.5K_BT$.

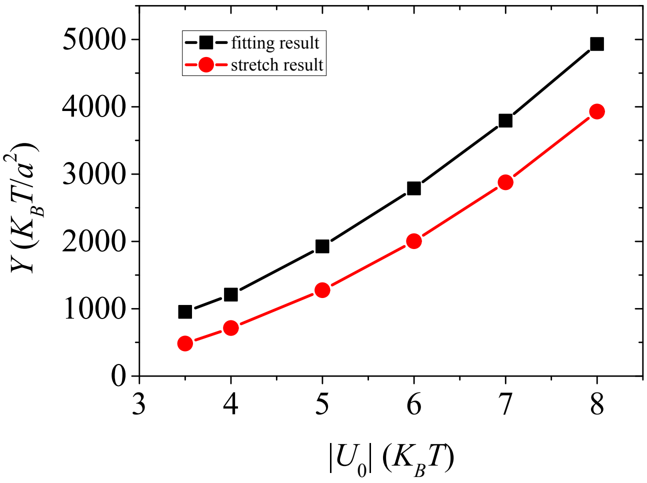

Figure S2 The relationship between Young's modulus Y versus different LJ potential strength $|U_0|$ at fixed crystal size $W/R = 0.3$ and curvature radius $R/a = 40$. The black dotted line is the fitting result and the red dotted line is the result from 2D stretching stress-strain curve as Figure 4 shows, respectively.

In the same way, the boundary force T of curved crystal in the Eqs. (2)(3) is fitted and plotted in Figure S3 at fixed $R/a = 40$ and $W/R = 0.3$. It is found that the boundary force is compressive stress ($T<0$) and its absolute value increases with the increase of LJ potential strength $|U_0|$. With the relationship $T = -\gamma/W$, Figure S4 shows the dependence of edge energy γ on $|U_0|$ at fixed $R/a = 40$ and $W/R = 0.3$.

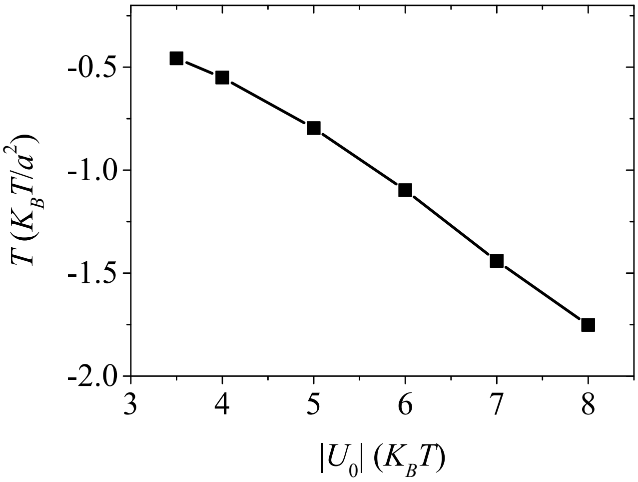

Figure S3 The dependence of boundary force T on the LJ potential strength $|U_0|$ at fixed $R/a = 40$ and $W/R = 0.3$.

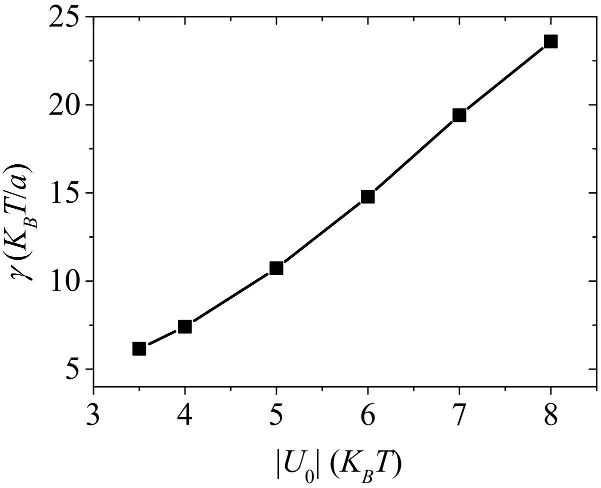

Figure S4 The dependence of edge energy γ on the LJ potential strength $|U_0|$ at fixed $R/a = 40$ and $W/R = 0.3$.

3. The relationships between dislocation density η with W/R and R/a

We define $\eta = M/4\pi R^2$ as the dislocation density of assembled crystals with M the number of dislocations. Figure S5 and Figure S6 shows the relationships between the dislocation density η with W/R and R/a, respectively. It is clear from Figure S5 that the dislocation density increases with the increase of W/R at the fixed substrate radius *R/a*=20 and minimal potential $|U_0| = 3.5K_BT$ when W/R reaches a critical value W/R=0.49. When area fraction W/R=0.89 and minimal potential $|U_0| = 3.5K_BT$ are fixed, the increase of *R/a* leads to a morphological transition from dislocation-decorated circular crystal shape to anisotropic growth of crystal, and the dislocation density decreases monotonously and finally reaches zero.

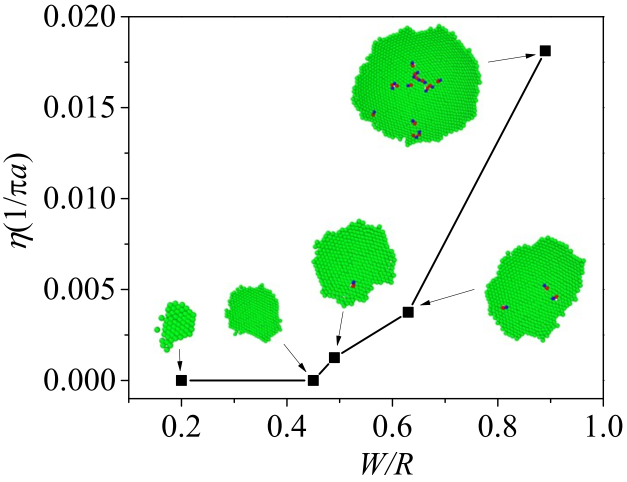

Figure S5 The dislocation density η of assemblies on spherical surfaces versus W/R for fixed *R/a*=20 and $|U_0| = 3.5K_BT$.

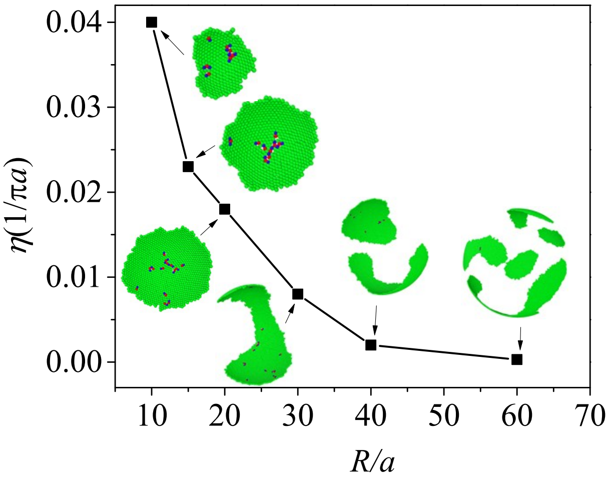

Figure S6 The dislocation density η of assemblies on spherical surfaces versus *R/a* for fixed

$$W/R = 0.89 \text{ and } |U_0| = 3.5K_BT \qquad .$$

4. The evolution sequences of the simulated results

Figure S7 shows the evolution sequences of the simulated results Fig. 6(e), Fig. 6(j) and Fig. 7(d) for different time steps. We find that the elastic instability which is encountered first will maintain its type during assembly process until the crystal reaches the kinetically stable state, although the crystal morphologies will evolve from the dispersed particles to compact crystal.

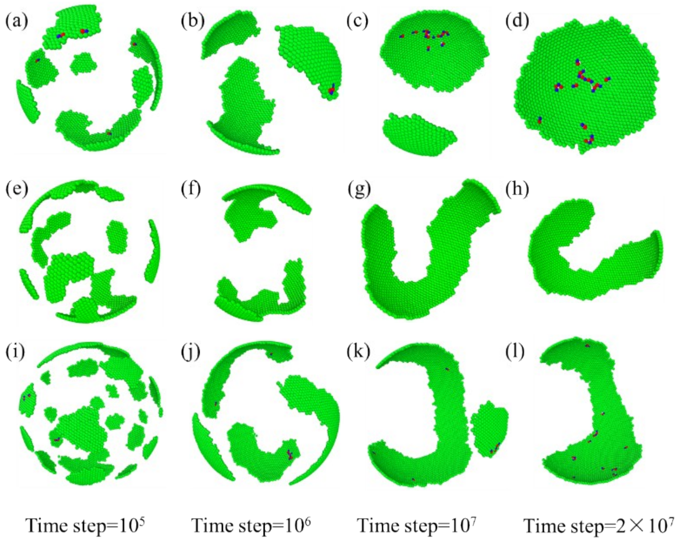

Figure S7 The evolution sequences of the simulated crystal morphologies for different time steps.

5. The stress configurations of the curved crystal cap in BD simulation and the fitting procedure

Using the Langevin thermostat at absolute zero temperature, we calculate the stress field of a constrained crystalline cap on spherical surface. Figure S8 shows the hoop stress distributions of the crystal caps for discrete particles under potential strength. It is obvious that the stress increases with the increase of potential strength. Given the symmetrical stress fields and the geometric parameter *W/R*, the Young's modulus Y and edge energy γ can be numerically fitting from the stress expression $\sigma^0_{\theta\theta}(r)=\frac{Y}{16R^2}\left(W^2-3r^2\right)-\frac{\gamma}{W}$. Figure S9 shows the comparison between the discrete stress field and the continuous elliptical paraboloid surface obtained by least square method. Except the simulated stress near the edge of crystal cap which shows major errors, the fitting method can well extract the features of the stress field.

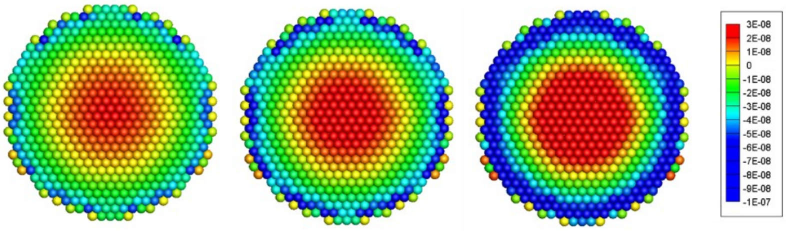

$|U_0|=3.5K_BT$ $|U_0|=4.0K_BT$ $|U_0|=5.0K_BT$

Figure S8 The hoop stress distributions of the crystal caps with the size of *R/a*=40 and *W/R*=0.3. Here the unit of the calculated 2D stress is N/m.

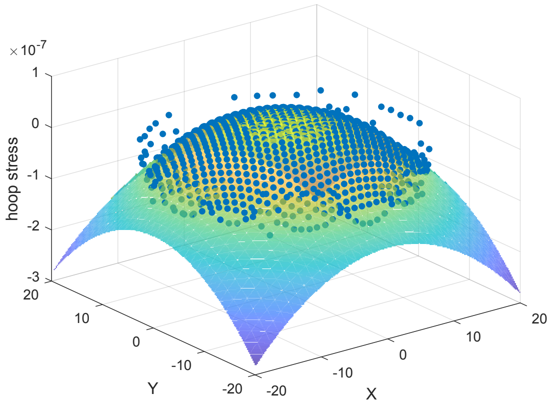

Figure S9 The numerically fitting of the discrete stress field. The size is *R/a*=40 and *W/R*=0.4, and the potential strength is $|U_0|=3.5K_BT$. Here the unit of the calculated 2D stress is N/m.

6. The calculation of the edge energy from a straightforward approach

To validate the reasonability of the values of edge energy from the fitting method, here we perform a straightforward approach for calculating the edge energy. First we create a monolayer structure with dimensions of $200a \times 400a$, as shown in Fig. S10(a). Starting from the initial 1.1225σ lattice spacing, we perform energy minimization for the 2D sheet. Then we separate the 2D sheet into two same-sized parts along *x* direction as Fig. S10(b) shows, and the system is fully relaxed. The edge energy of the 2D LJ crystal is calculated by $\gamma_{cut} = \left(E_{cut} - E_{initial}\right)/2l_x$, where $E_{initial}$ and E_{cut} are the minimum potential energies for the configurations in Figs. S10 (a) and (b), respectively, and l_x is the length of the 2D sheet in *x* direction. Periodical boundary conditions are applied in the calculation. The difference between the two methods is that the "cutting" method is a straightforward approach to calculate the energy increasing per unit length when separating a 2D sheet along a line of known length, while the fitting method in this work employs the edge effect on the 2D elasticity encoded by the relationship of $\sigma_{ij}n_j = -\gamma C(\theta)n_i$ as the boundary condition and fits the edge energy γ from the stress distribution of the curved crystal. We must say that there is no difference between γ and γ_{cut} which both represent the edge energy. However the fitting method to determine the value of γ is an indirect method in comparison with the determination of γ_{cut}. The results in Fig. S11 confirm that the values of the edge energy γ obtained by two different methods are almost the same. It means that the fitting edge energy from the stress distribution in this work is reliable.

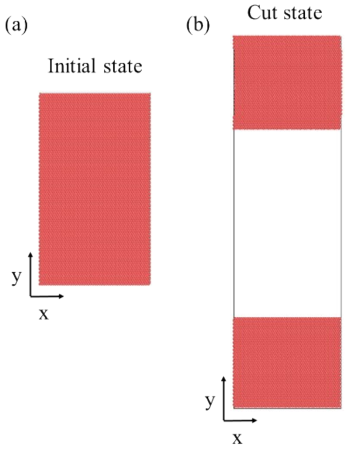

Fig. S10 The schematic diagram of separating a 2D sheet along *x* direction.

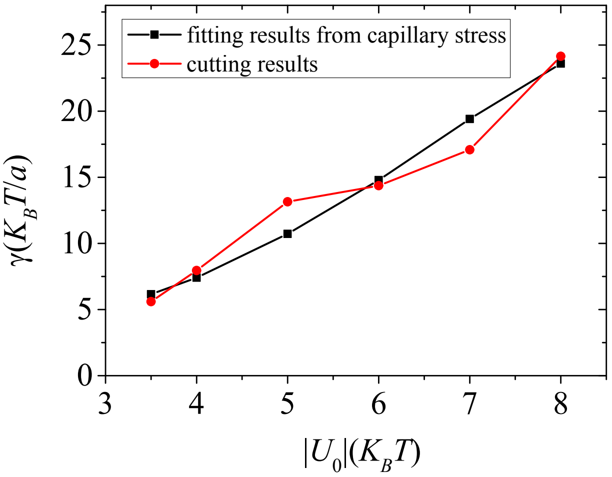

Fig. S11 The dependence of the edge energy on the potential strength. The results in red color are obtained by the "cutting" method, and the results in black color are fitted from the stress distribution of curved crystal at fixed $R/a = 40$ and $W/R = 0.3$.

1. Asaro, R.; Tiller, W. *Metallurgical Transactions* **1972,** 3, (7), 1789-1796.
2. Morozov, A. Y.; Bruinsma, R. F. *Phys. Rev. E* **2010**, 81, (4), 041925.